The inhibition of LSD1 via sequestration contributes to tau-mediated neurodegeneration

Amanda K. Engstrom[1], Alicia C. Walker[1], Rohitha A. Moudgal[1], Dexter A. Myrick[1], Stephanie M. Kyle[1], David J. Katz[1*]

[1] Department of Cell Biology, Emory University School of Medicine, Atlanta GA 30322, USA.

*Correspondence to: David J, Katz Email: djkatz@Emory.edu.

ABSTRACT

Tauopathies are a class of neurodegenerative diseases associated with pathological tau. However, the mechanism through which tau contributes to neurodegeneration remains unknown. Previously, our lab implicated the histone demethylase LSD1 in tau-induced neurodegeneration by showing that LSD1 localizes to pathological tau aggregates in Alzheimer's disease cases, and that it is continuously required for the survival of hippocampal and cortical neurons in mice. Here, we utilize the P301S tauopathy mouse model to demonstrate that pathological tau can exclude LSD1 from the nucleus in neurons. In addition, we show that reducing LSD1 in these mice is sufficient to highly exacerbate tau-mediated neurodegeneration. Finally, we find that overexpressing LSD1 in the hippocampus of tauopathy mice, even after pathology has formed, is sufficient to significantly delay neurodegeneration. These results suggest that inhibiting LSD1 via sequestration contributes to tau-mediated neurodegeneration. Thus, LSD1 is a promising therapeutic target for tauopathies such as Alzheimer's disease.

INTRODUCTION

Tauopathies such as corticobasal degeneration, progressive supranuclear palsy, and frontotemporal lobar degeneration with tau inclusions are neurodegenerative diseases pathologically defined by different forms of tau positive intraneuronal deposits (*1-5*). In addition to these primary tauopathies, neuropathological observations of postmortem Alzheimer's disease (AD) brains show the presence neurofibrillary tangles (NFTs) of hyperphosphorylated tau protein, as well as plaques containing β-amyloid (Aβ) peptide (*6-9*). AD is the leading cause of age-related dementia, resulting from neuronal cell death in the frontal and temporal cortices, as well as the hippocampus (*7*). As dementia progresses, the spatial pattern of tau pathology highly correlates with the level of cognitive impairment (*10-13*). In addition, Aβ oligomers and/or plaques can enhance tau pathology in various mouse models (*24, 25*), and there is increasing evidence that accumulation of Aβ plaques can contribute to tau pathology (*3, 26, 27*). The most well-defined physiological role of tau is in stabilizing microtubules, particularly in neuronal axons (*2*). However, in the pathological state, tau becomes aberrantly phosphorylated (*2, 14, 15*), truncated (*1, 4*), and aggregates into oligomers and larger insoluble filaments (*16, 17*). This pathology is thought to trigger synaptic loss, dramatic genome-wide expression changes, increased inflammatory response, and neuronal cell death (*18-21*). These data suggest that pathological tau may be a downstream mediator of the neurotoxic effects leading to neuronal degeneration in AD.

Previously, our lab demonstrated that deleting the histone demethylase *Lsd1* in adult mice leads to significant neuronal cell death in the hippocampus and cortex with associated learning and memory defects (*28*). In this mouse model, loss of *Lsd1* induces genome-wide expression changes that significantly overlap with those observed in the brains of postmortem human AD

49 cases, but not other neurodegenerative diseases, such as Parkinson's disease or amyotrophic
50 lateral sclerosis (ALS) cases. Consistent with this overlap, we observed LSD1 protein
51 mislocalized to cytoplasmic NFTs, but not associated with Aβ plaques in AD cases or Lewy
52 bodies of α-synuclein in Parkinson's disease cases (*28*). These data highlight the requirement for
53 LSD1 in neuronal survival and suggest that the nuclear function of the histone demethylase
54 LSD1 could be disrupted by mislocalization to pathological tau.

55 To investigate how LSD1 may contribute to tau-mediated neurodegeneration, we utilized
56 the PS19 P301S tauopathy mouse model (hereafter referred to as PS19 Tau). PS19 Tau mice
57 express a P301S mutated form of the human tau protein, originally identified in a frontotemporal
58 dementia with parkinsonism (FTDP-17) patient, driven by the prion promoter throughout the
59 nervous system (*29*). When expressed in mice, the P301S tau protein is prone to
60 hyperphosphorylation and somatodendritic aggregation, without the presence of Aβ plaques.
61 PS19 Tau mice develop a heavy pathological tau burden and have been well characterized for the
62 temporal progression of tau pathology and disease-related phenotypes (*30, 31*). However, the
63 mechanism of neuronal cell death caused by pathological tau is still unknown.

64 Here, we provide functional data that the inhibition of LSD1 function contributes to tau
65 induced neurodegeneration. We demonstrate in PS19 Tau mice that pathological tau sequesters
66 LSD1 in the cytoplasm of neurons throughout the brain. This results in depletion of LSD1 from
67 the nucleus. Additionally, we provide genetic and molecular evidence that pathological tau
68 contributes to neurodegeneration by disrupting LSD1. Finally, we show that overexpressing
69 LSD1 in hippocampal neurons is sufficient to suppress neuronal cell death even after
70 pathological tau has formed. We propose that pathological tau contributes to neuronal cell death

71 by sequestering LSD1 in the cytoplasm, depleting the nuclear pool of LSD1 that is required for
72 neuronal survival.
73
74 **RESULTS**
75 **Tau pathology depletes LSD1 from the nucleus in the PS19 Tau mouse model**
76 Previously, we showed in human AD cases that LSD1 protein inappropriately colocalizes with
77 NFTs in the cell body of hippocampal and cortical neurons, while in unaffected controls LSD1
78 was properly localized exclusively to the nucleus (*28*). However, because neurons in AD cases
79 with intracellular NFTs presumably die and are cleared, it was difficult to determine whether tau
80 prevents LSD1 from localizing to the nucleus in a dying neuron. To address this possibility, we
81 performed LSD1 immunofluorescence on 12 month old PS19 Tau mice, which have significant
82 tau pathology (*29*). Because PS19 Tau mice undergo neurodegeneration over a shortened period,
83 there are more neurons undergoing neurodegeneration at any given time point. Thus, we
84 reasoned that it may be possible to observe LSD1 depletion from the nucleus. Similar to what we
85 observe in humans, LSD1 protein in 12 month old Wild Type mice was localized to the nucleus
86 of neurons in the cerebral cortex (Fig. 1A-C) and the hippocampus (Fig. S1 A-C). However, in
87 12 month old PS19 Tau mice, LSD1 protein was sequestered in the cytoplasm and depleted from
88 the nucleus both in the cerebral cortex (Fig. 1D-F) and the hippocampus (Fig. S1 D-F). These are
89 both regions where we observe substantial cytoplasmic tau pathology (Fig. 1G-I; Fig. S1 G-I).
90 Similarly, in other brain regions that accumulate tau pathology, such as the thalamus and
91 amygdala, LSD1 was localized to the nucleus in 12 month old Wild Type control mice (Fig. S1
92 J-O), but abnormally localized to the cytoplasm in PS19 Tau mouse littermates (Fig. S1 P-U).
93 Overall, we observed sequestration of LSD1 in 6 out of 7 mice analyzed. In each of the 6 mice,

94 there were varying levels of sequestration ranging from LSD1 found in both the nucleus and
95 cytoplasm (Fig. S1 V-X), to depletion from the nucleus (Fig. S1 Y-DD).
96
97 **Reduction of LSD1 increases the mouse tauopathy phenotype**
98 If the presence of pathological tau in the cytoplasm is leading to neuronal cell death through the
99 sequestration and nuclear depletion of LSD1, we would expect that lowering the overall levels of
100 LSD1 would accelerate depletion and exacerbate the progression of disease. To test this, we
101 made PS19 Tau mice heterozygous for *Lsd1* (hereafter referred to as PS19;*Lsd1*$^{\Delta/+}$, Fig. S2 A).
102 *Lsd1* heterozygotes (hereafter referred to as *Lsd1*$^{\Delta/+}$) have a functioning copy of *Lsd1* and don't
103 have phenotypes associated with LSD1 loss of function (*32-34*). Thus, *Lsd1* heterozygosity does
104 not completely compromise LSD1 function. Instead mice that are heterozygous for *Lsd1* are
105 sensitized to mechanisms affecting LSD1 localization and function. Consistent with this, we
106 observed a 30% reduction in transcript levels (Fig. S2 B) and a 35% reduction in protein levels
107 (Fig. S2 C,D) in *Lsd1*$^{\Delta/+}$ mice compared to their *Lsd1*$^{+/+}$ littermates. Surprisingly, PS19 Tau mice
108 have a 20% increase in LSD1 protein levels compared to *Lsd1*$^{+/+}$ littermates. Nevertheless,
109 consistent with the reduction in LSD1 that we observe in *Lsd1*$^{\Delta/+}$ mice, PS19;*Lsd1*$^{\Delta/+}$ mice have
110 a similar 26% reduction in transcript levels (Fig. S2 B) and a 31% reduction in protein levels
111 (Fig. S2 C,D) compared to PS19 Tau littermates. In addition, all genotypes were born at normal
112 Mendelian ratios with equal male/female ratios.
113 As expected, *Lsd1*$^{\Delta/+}$ mice had normal survival (Fig. 2A). In contrast, PS19 Tau mice had
114 a reduced overall survival (Fig. 2A) (*29*). When one copy of *Lsd1* was removed from PS19 Tau
115 mice, their reduced survival was significantly exacerbated (P-value = 0.0017, Fig. 2A). As
116 expected, there was little effect on the onset of reduced viability. The initial decline in the

117 survival of PS19;*Lsd1*$^{\Delta/+}$ mice started only slightly earlier than PS19 Tau mice, but after the
118 appearance of pathological tau in neurons (Fig. S6 K-M) (*29*). This suggests that pathological tau
119 may have to be present before *Lsd1* heterozygosity has deleterious effects. Subsequently,
120 PS19;*Lsd1*$^{\Delta/+}$ mice had a 14% reduction in median lifespan compared to PS19 Tau mice and
121 reached median survival 44 days earlier then PS19 Tau mice. In addition, there was a further
122 exacerbation of reduced lifespan as pathology became more severe. PS19;*Lsd1*$^{\Delta/+}$ mice reached
123 the point when there was only 10% of the population remaining 83 days earlier than PS19 Tau
124 mice, and all but one of the last 25% of PS19;*Lsd1*$^{\Delta/+}$ mice died between 11.5-13.5 months,
125 compared to 13.5-19 months in PS19 Tau mice. As a result, 28% of PS19 Tau mice were still
126 alive after all but one of the PS19;*Lsd1*$^{\Delta/+}$ mice had died (Fig. 2A).

127 PS19 Tau mice develop paralysis starting with hind limb clasping which progresses until
128 they are unable to feed (*29*). In our hands, PS19 Tau mice displayed intermittent hind limb
129 clasping starting at approximately 6 months of age. At 12 months, these mice had a severe clasp,
130 but were still mobile. This is delayed compared to what was originally reported by Yoshiyama
131 and colleagues (*29*). PS19;*Lsd1*$^{\Delta/+}$ mice also displayed intermittent hind limb clasping beginning
132 at approximately 6 months of age. However PS19;*Lsd1*$^{\Delta/+}$ mice became terminally paralyzed at a
133 faster rate compared to PS19 Tau mouse littermates. At 12 months, when PS19 Tau mice were
134 still mobile, PS19;*Lsd1*$^{\Delta/+}$ mice were severely paralyzed and typically terminal (Movie S1). To
135 quantitatively assess paralysis we performed rotarod and grid performance tests. In the rotarod,
136 we assessed the ability of the mice to stay on the rotating rod (latency to fall) (Fig. 2B), the speed
137 of the rod at which they fall off the rotarod (rotations per minute) (Fig. 2C), and the total distance
138 traveled (Fig. 2D). All genotypes performed the same at 6 months and 8 months (Fig. 2B-D).
139 However, at 10 months, when PS19 Tau mice still performed normally, PS19;*Lsd1*$^{\Delta/+}$ mice had a

140 significant deficit in mobility (P-value < 0.01, Fig. 2B,C). A deficit in PS19;*Lsd1*$^{\Delta/+}$ mice was
141 also observed at 10 months in the total distance traveled (Fig. 2D) and in grid performance
142 testing (Fig. S3 A), though neither were statistically significant.

143 To further investigate the exacerbation of paralysis we examined the spinal cord motor
144 neurons. Healthy motor neurons from *Lsd1*$^{+/+}$ control mice express LSD1 (Fig. S3 B-D) and are
145 classically identified by circular nuclei at the center of a large cell body. In contrast to the
146 healthy motor neurons we observed in 12 month old PS19 Tau mice (Fig. S3 E), many of the
147 motor neurons in PS19;*Lsd1*$^{\Delta/+}$ mice at 12 months had abnormal morphology, with the nucleus
148 skewed to the edge of the cell body (Fig. S3 E vs. S3 F) and a ballooned cell body (Fig. S3 F).
149 Within the cell body we found aberrant hyperphosphorylated NFH (heavy chain neurofilament),
150 which is a sign of activated neuronal stress pathways (Fig S3 G vs. S3 H) (*35, 36*). This
151 abnormal morphology is highly reminiscent of a well-established process known as
152 chromatolysis, which is characterized by swelling of the neuronal cell body, disruption of Nissl
153 granules, and pyknotic or shrunken nuclei abnormally skewed to the edge of the cell body (*37,*
154 *38*). Chromatolysis, which is linked to neuronal stress and often leads to apoptosis (*38*), has been
155 observed in AD and other neurodegenerative diseases (*37, 39-41*).

156

157 **Reduction of LSD1 exacerbates PS19 Tau neurodegeneration**

158 In addition to accelerating the paralysis phenotype, reducing the level of *Lsd1* in PS19 Tau mice
159 exacerbated neuronal cell death in the brain. At 6 months and 8 months, we observed no
160 difference between genotypes in the overall morphology in the hippocampus (Fig. S4 A-H)
161 based on histological analysis. There was also no difference between *Lsd1*$^{+/+}$ and *Lsd1*$^{\Delta/+}$ mice at
162 10 months or 12 months (Fig. 3A,B; Fig. S4 I,J,M,N; Fig. S5 A,B,E,F,I,J,M,N). At 10 months,

163 PS19 Tau mice had very little cell loss in the hippocampus compared to *Lsd1*$^{+/+}$ and *Lsd1*$^{\Delta/+}$
164 control mice (Fig. S4 I-K, M-O). In contrast, at 10 months, PS19;*Lsd1*$^{\Delta/+}$ mice had dramatic cell
165 loss both in the CA1 region of the hippocampus and throughout the posterior hippocampus (Fig.
166 S4 L,P). At 12 months, the PS19 Tau mice had a slight decrease in CA1 and CA3 neurons
167 spanning the hippocampal pyramidal cell layer compared to *Lsd1*$^{+/+}$ control mice (17% and
168 19.4% respectively, Fig. 3A,B; Fig. S5 A-C, E-G). In comparison, PS19;*Lsd1*$^{\Delta/+}$ mice had a 52%
169 and 54% decrease in the CA1 and CA3 respectively (Fig. 3A,B; Fig. S5 D,H) compared to
170 *Lsd1*$^{+/+}$ control mice. This resulted in decreased overall brain size (Fig. 3C) and brain weight
171 (Fig. 3D) in PS19;*Lsd1*$^{\Delta/+}$ mice compared to PS19 Tau and *Lsd1*$^{\Delta/+}$ mouse littermates.
172 Additionally, at 12 months there were increased levels of cell loss in the Dentate Gyrus (Fig. S5
173 I-L), and throughout the posterior hippocampus (Fig. S5 M-P).
174 Along with the histology, we monitored the progression of neuronal cell death in the
175 same individual over time by performing magnetic resonance imaging (MRI) at 6 months and
176 again at 10 months (Movie S2). At 6 months, there was no sign of cell loss or ventricular
177 dilatation in *Lsd1*$^{\Delta/+}$, PS19 Tau, or PS19;*Lsd1*$^{\Delta/+}$ mice (Fig. 3E-G). However, at 10 months the
178 MRI showed that there was dramatic ventricular dilatation in PS19;*Lsd1*$^{\Delta/+}$ mice, as evidenced by
179 high-intensity areas in T2- weighted imaging, with substantial hippocampal and neocortical
180 atrophy (Fig. 3J vs. 3H, Movie S2). At this timepoint, PS19 Tau mice had some ventricular
181 dilatation and hippocampal atrophy throughout the hippocampus (Fig. 3I), but much less than
182 PS19;*Lsd1*$^{\Delta/+}$ mice (Fig. 3J, Movie S2. 0:51sec vs. 1:00sec).
183
184 **Tau pathology is not affected by change in LSD1 levels**

185 Since LSD1 is a chromatin regulator, it is possible that reducing LSD1 protein levels affects the
186 PS19 Tau transgene. However, we confirmed that there was no difference between PS19 Tau
187 mice and PS19;*Lsd1*$^{\Delta/+}$ mice in the endogenous mouse *Mapt* RNA expression, nor in the human
188 P301S MAPT transgene expression (Fig. S6 A). It is also possible that LSD1 affects tau
189 pathology. To test this, we performed immunohistochemistry staining for a hyperphosphorylated
190 form of tau (AT8). As expected, we did not observe any AT8 positive staining in *Lsd1*$^{\Delta/+}$ at 6, 8,
191 or 10 months (Fig. S6 B,E,H). Additionally, we observed very little AT8 positive
192 immunoreactivity at 6 months in both PS19 Tau or PS19;*Lsd1*$^{\Delta/+}$ mice (Fig. S6 C,D). At 8
193 months both PS19 Tau and PS19;*Lsd1*$^{\Delta/+}$ mice had low but consistent levels of AT8 positive
194 immunoreactivity (Fig. S6 F,G), and by 10 months both PS19 Tau and PS19;*Lsd1*$^{\Delta/+}$ mice
195 developed the same high level of AT8 positive tau immunoreactivity (Fig. S6 I,J). This was
196 consistent throughout both the CA1 and CA3 regions of the hippocampus and the cerebral cortex
197 (Fig. S6 K-M). We also did not observe any difference between PS19 Tau mice and
198 PS19;*Lsd1*$^{\Delta/+}$ mice when assaying PHF1 (an alternative phospho-tau antibody) immunoreactivity
199 in the CA1 region of the hippocampus at 8 months (Fig. S7 A-C, G) and 10 months (Fig. S7 D-F,
200 G), nor in the CA3 region of the hippocampus or the cerebral cortex at 8 and 10 months (Fig. S7
201 H,I).
202

203 **The functional interaction between tau pathology and LSD1 inhibition is specific**

204 To test the specificity of the functional interaction between tau pathology and LSD1, we
205 investigated the overlap in the effected molecular pathways associated with both pathological tau
206 and *Lsd1* heterozygosity. To address this, we performed RNA sequencing on the hippocampus of
207 9 month *Lsd1*$^{+/+}$, *Lsd1*$^{\Delta/+}$, PS19 Tau, and PS19;*Lsd1*$^{\Delta/+}$ littermates. As opposed to analyzing

208 transcriptional changes at the terminal stage of disease, this time point allows us to assess
209 molecular changes prior to the onset of neuronal cell death. This is also the time point that we
210 observed the earliest signs of exacerbation of paralysis in PS19;*Lsd1*$^{\Delta/+}$ mice. Because of this
211 early stage in the progression of the disease, we would not expect dramatic changes in
212 transcription overall. Nevertheless, if tau pathology is inhibiting LSD1 function, we would
213 expect that the genome-wide expression changes induced by tau might be exacerbated by a
214 reduction in LSD1. The RNA-seq analysis detected 54 significant gene expression changes in
215 PS19 Tau mice compared to *Lsd1*$^{+/+}$ (Fig S8 A,B), and 271 significant gene expression changes
216 in PS19;*Lsd1*$^{\Delta/+}$ mice compared to *Lsd1*$^{+/+}$ (Fig S8 C,D). Importantly, *Lsd1*$^{\Delta/+}$ mice had only 4
217 gene expression changes observed genome-wide (Fig. S8 E,F), indicating that the partially
218 reduced level of LSD1 expression had very little effect on transcription on its own. This is
219 consistent with the lack of phenotype in these animals.

220 We first examined the relationship between tau-induced expression changes and the
221 effects of *Lsd1* heterozygosity by comparing the transcriptional changes observed in PS19 Tau
222 mice with PS19;*Lsd1*$^{\Delta/+}$ mice. In PS19 Tau mice that do not yet have significant
223 neurodegeneration, we identified 54 genes (36 up and 18 down) that were differentially
224 expressed. Of these 54 genes, 50 were changed in the same direction in PS19;*Lsd1*$^{\Delta/+}$ mice
225 (93%). In addition, amongst the 50 genes changed in the same direction, 36 (72%) had
226 exacerbated expression in PS19;*Lsd1*$^{\Delta/+}$ mice compared to PS19 Tau mice (Fig. 4A). Based on
227 this overlap, we further compared the expression changes between PS19 Tau mice and
228 PS19;*Lsd1*$^{\Delta/+}$ mice genome-wide. Amongst the transcripts that were changed in both PS19 Tau
229 mice and PS19;*Lsd1*$^{\Delta/+}$ mice compared to *Lsd1*$^{+/+}$ mice, 71% changed in the same direction
230 (either up or down). Consistent with this overlap in gene expression, Gene Set Enrichment

231 Analysis demonstrated that the pathways that are affected in both PS19 Tau mice and
232 PS19;*Lsd1*$^{\Delta/+}$ mice are very similar (Fig. S8 G-J). However, the genes affected in both sets of
233 mice tended to be further exacerbated in PS19;*Lsd1*$^{\Delta/+}$ mice compared to PS19 Tau mice.
234 Amongst the 71% of genes that changed in the same direction in both PS19 Tau mice and
235 PS19;*Lsd1*$^{\Delta/+}$ mice, 76% of these transcripts had a higher fold-change in PS19;*Lsd1*$^{\Delta/+}$ mice
236 compared to PS19 Tau mice (Fig. 4B).
237
238 **Overexpression of LSD1 rescues neurodegeneration in the hippocampus of PS19 Tau mice**
239 Our data demonstrate that reduction of LSD1 protein exacerbates the tauopathy phenotype in
240 PS19 Tau mice. Based on this, we considered the possibility that overexpression of LSD1 might
241 counter the loss of LSD1 from the nucleus and protect against neurodegeneration in PS19 Tau
242 mice. To address this possibility, we injected PS19 Tau mice with a neuronal specific virus
243 (AAV-DJ driven by the synapsin promoter) expressing either the full length LSD1 protein with
244 an N-terminal HA tag (hereafter referred to as PS19- LSD1 inj) or a control virus expressing
245 only the HA tag (hereafter referred to as PS19- HA inj). Additionally, to control for the effects of
246 viral injection, we injected Wild Type littermates with the HA only expressing virus (hereafter
247 referred to as WT- HA inj). All injections were performed directly into the hippocampus at 8-8.5
248 months, when tau pathology is already present throughout the nervous system. Immunolabeling
249 for the HA tag demonstrated that the virus is specific to NeuN+ neurons (Fig. S9 A-D), with no
250 HA expression observed in IBA+ microglia (Fig. S9 E-H), or GFAP+ astrocytes (Fig. S9 I-L). It
251 also confirmed that virally expressed LSD1 is nuclear (Fig. S9 M) and confined to the
252 hippocampus (Fig. S9 N). After 3 months of overexpression, 11-11.5 month old mice were
253 euthanized, and the brains were analyzed. Injections resulted in a ~6-fold increase in expression

254 of LSD1 in the hippocampus compared to endogenous LSD1 in the PS19- HA inj mice, but no
255 increase in the cerebellum (Fig. S9 O,P). As expected, because the viral injections were restricted
256 to the hippocampus, the mice injected with LSD1 still developed paralysis (Movie S3). This
257 confirms that the tau transgene is expressed and functioning. Additionally, we did not observe a
258 difference in total levels of AT8 positive tau immunoreactivity (Fig. S9 Q-T). Therefore, any
259 modulation to the phenotype was not due to changes in tau pathology.

260 Injected mice were evaluated for cell death by neuronal cell counts in the hippocampus.
261 Injection of LSD1 virus into the hippocampus of PS19 Tau mice rescued the neurodegeneration
262 phenotype. At 11 months, compared to WT-HA inj control mice, 70% of the PS19-HA inj mice
263 had hippocampal cell counts that were below the lowest WT-HA inj control, while none of the
264 Tau mice injected with the LSD1 virus were below this level. Overall, we observed significantly
265 more neurons (P-value <0.05) spanning the pyramidal cell layer (84% of WT- HA inj CA1
266 counts) compared to their PS19- HA inj littermates (59% of WT- HA inj CA1 counts), such that
267 overall the neuronal cell count in PS19- LSD1 inj mice was not statistically different from the
268 WT- HA inj (Fig. 5A-D). Additionally, in the histological analysis we observed a large number
269 of cells infiltrating the hippocampus in PS19- HA inj mice compared to WT- HA inj littermates
270 (Fig. 5B vs. 5C). Marker analysis demonstrated that this was due to a strong inflammatory
271 response, with a large increase in the number of GFAP+ astrocytes (Fig. S10 A-C vs. D-F) and
272 TRL2+ activated microglia (Fig. S10 J-L vs. M-O, S-V vs. W,Z, EE). Injection of PS19 Tau
273 mice with LSD1 virus rescued this inflammatory response. For example, all but one (9 out of 10
274 analyzed) of the PS19- LSD1 inj mice had a reduction in the number of GFAP+ astrocytes (Fig.
275 S10 G-I vs. D-F) and TRL2+ activated microglia (Fig. S10 P-R vs. M-O, AA-DD vs. W-Z, EE).
276 Of note, the one PS19- LSD1 inj mouse where we did observe increased glial cells, similar to

277 PS19- HA inj mice, had the lowest neuronal cell count (74% of WT- HA inj CA1 neurons). It is
278 possible that this mouse was already undergoing neurodegeneration prior to the injection of the
279 LSD1 overexpression virus.

280 Although the number of hippocampal neurons in PS19- LSD1 inj mice did not differ
281 from WT- HA inj controls, in 6 of the 10 PS19- LSD1 inj mice we observed cells with abnormal
282 blebbed nuclei at varying numbers throughout the hippocampus (Fig. 5E). These abnormal cells
283 are rare in PS19- HA inj mice, which have a reduced overall number of cells in the pyramidal
284 cell layer compared to WT- HA inj control mice. One possibility is that these abnormal cells
285 with blebbing nuclei represent an intermediate state between a healthy neuron and a dying
286 neuron that is prolonged by rescue via LSD1 overexpression. Interestingly, these abnormal cells
287 also differed in the localization of HA-tagged LSD1. The four mice with normal nuclei had HA-
288 tagged LSD1 protein localized uniformly throughout the nucleus (Fig. 5F). In contrast, the six
289 mice with abnormal nuclear blebbing had some HA-tagged LSD1 that was mislocalized to the
290 cytoplasm (Fig. 5G). This includes the one PS19- LSD1 inj mouse that had an elevated number
291 of astrocytes and TRL2 positive microglia. Thus, the blebbing state correlates with when the
292 viral produced LSD1 begins to be sequestered in the cytoplasm, similar to the endogenously
293 produced LSD1.

294

295 **DISCUSSION**

296 In this study we investigate a potential downstream mediator of tau pathology in
297 neurodegenerative disease. We find that modulation of the chromatin modifying enzyme LSD1
298 can alter neurodegeneration in a tauopathy mouse model. Previously, we showed that LSD1
299 colocalizes with tau pathology in the cell body of neurons in AD cases (*28*). This suggested that

300 LSD1 might be disrupted in tauopathies such as AD, by being excluded from the nucleus. To
301 address this directly, we utilize the PS19 tauopathy mouse model. In these mice, we find that
302 LSD1 is sequestered in the cytoplasm, in some cases being completely depleted from the
303 nucleus. This provides the first cytological evidence that pathological tau can prevent LSD1 from
304 properly localizing to the nucleus in hippocampal and cortical neurons, where we have
305 previously shown it is continuously required.

306 Based on the ability of pathological tau to sequester LSD1, we hypothesized that
307 neuronal cell death may be due, at least partly, to LSD1 being sequestered in the cytoplasm and
308 depleted from the nucleus. In this case, reducing LSD1 levels should make it easier for tau to
309 deplete LSD1 from the nucleus, resulting in a faster progression of neurodegeneration and/or a
310 more severe neurodegenerative phenotype. Importantly, LSD1 heterozygosity alone induces only
311 4 significant gene expression changes and does not lead to any neurodegeneration. This suggests
312 that any effects observed in PS19;*Lsd1*$^{\Delta/+}$ mice are not simply due to LSD1 haploinsufficiency.
313 Normally, PS19 Tau mice develop paralysis and neurodegeneration, along with reduced survival.
314 In contrast, when we reduce LSD1 in the PS19 Tau mice, PS19;*Lsd1*$^{\Delta/+}$ mice die significantly
315 earlier, most likely due to the increased rate of paralysis. Additionally, PS19;*Lsd1*$^{\Delta/+}$ mice have
316 increased neuronal cell death and clearance in the hippocampus. This suggests that pathological
317 tau functions through LSD1 to cause neurodegeneration *in vivo* in mice.

318 PS19;*Lsd1*$^{\Delta/+}$ mice have a 31% reduction in LSD1 protein levels compared to PS19 Tau
319 mice from birth. This reduction should theoretically make mice sensitive to LSD1 depletion at
320 any time. However, tau pathology starts at 6-8 months in PS19 Tau mice. As a result, if *Lsd1*
321 heterozygosity is functioning by making it easier for pathological tau to deplete LSD1 from the
322 nucleus, we would not expect to see any exacerbation until after pathological tau is present. The

323 exacerbation of the PS19 Tau mouse neurodegenerative phenotype does not occur until after
324 pathological human tau was present. This suggests that the effect of *Lsd1* heterozygosity requires
325 the presence of pathological tau, placing LSD1 downstream of tau. Consistent with LSD1 being
326 downstream of pathological tau, we found no evidence that *Lsd1* heterozygosity affects the
327 expression of the tau transgene, or the buildup of pathological tau in PS19 Tau mice.

328 To test whether the functional interaction between pathological tau and reduced LSD1 is
329 specific, we used RNA-seq to determine whether the downstream molecular pathways altered in
330 PS19 Tau mice are exacerbated in PS19;*Lsd1*$^{\Delta/+}$ mice. This analysis was performed at the time of
331 earliest signs of neuronal distress, allowing us to assess molecular changes prior to cell death and
332 clearance. LSD1 heterozygosity induces only 4 significant expression changes. In addition, the
333 pathways are affected in both PS19 Tau mice and PS19;*Lsd1*$^{\Delta/+}$ mice are very similar. This
334 suggests that reducing LSD1 did not induce any additional neurodegeneration pathways. In
335 contrast, when LSD1 is reduced in PS19 Tau mice, the genome-wide expression changes
336 induced by pathological tau are specifically exacerbated. This suggest that the functional
337 interaction that we observe between pathological tau and reduced LSD1 is occurring through the
338 tau pathway.

339 Our previous data implicated LSD1 in the tau-mediated neurodegeneration pathway.
340 Utilizing the PS19 Tau mouse model, we now show a functional interaction between
341 pathological tau and LSD1. Importantly, because PS19 Tau mice do not have Aβ plaque
342 accumulation, this functional interaction is specific to tau. Based on these data we propose the
343 following model (Movie S4): in healthy hippocampal and cortical neurons, LSD1 is translated in
344 the cytoplasm and transported into the nucleus where it is continuously required to repress
345 inappropriate transcription. In tauopathy, pathological tau accumulates in the cytoplasm blocking

346 LSD1 from nuclear import. This interferes with the continuous requirement for LSD1, resulting
347 in neuronal cell death. Recently, it has been observed that the nuclear pore breaks down in AD
348 (*42-44*). It should be noted that this mechanism would potentially exacerbate the model that we
349 propose.

350 This model makes a direct prediction: if tau is predominantly functioning through LSD1,
351 then increasing the levels of LSD1 should rescue the tau-induced neurodegenerative phenotype.
352 To address this, we overexpressed LSD1 in the hippocampal neurons of PS19 Tau mice.
353 Overexpression of LSD1 specifically in hippocampal neurons rescues the neuronal cell death and
354 limits the inflammatory response. This rescue is neuronal specific, suggesting that the functional
355 interaction between LSD1 and tau is occurring in neurons. In addition, this rescue occurs despite
356 there being no effect on tau aggregation. This negates the possibility that the tau transgene is
357 simply not functioning when LSD1 is overexpressed. The ability of LSD1 overexpression to
358 overcome tau-mediated neurodegeneration in the presence of pathological tau aggregates,
359 provides further evidence that pathological tau is functioning through the inhibition of LSD1.
360 Importantly, overexpressing LSD1 should not prevent it from being sequestered. Rather
361 overexpressing LSD1 should make it more difficult for pathological tau to sequester all of the
362 LSD1 protein, allowing some LSD1 to be transported to the nucleus. Thus, overexpressing LSD1
363 would be expected to temporarily rescue the ability of pathological tau to kill neurons.
364 Consistent with this, LSD1 overexpression delays the effect of pathological tau rather than
365 permanently rescuing. In 60% of the mice, the surviving neurons have abnormal morphology,
366 and the overexpressed version of LSD1 is also sequestered. observation that neurons fail to
367 maintain their morphology when the overexpressed LSD1 begins to be sequestered in the
368 cytoplasm provides further support for the model that tau mediates neurodegeneration through

369 the sequestration of LSD1. Nevertheless, our data suggest that overexpression of LSD1 cannot
370 permanently overcome pathological tau. To permanently overcome pathological tau, it would
371 likely be necessary to permanently disrupt the interaction between pathological tau and LSD1.
372 This work is currently ongoing in the lab. Overall, our data establish LSD1 as a major
373 downstream effector of tau-mediated neurodegeneration. Based on these data, we propose that
374 the LSD1 pathway is a potential late stage target for intervention in tauopathies, such as AD.

375

376 **MATERIALS AND METHODS**

377 All mouse work, including surgical procedures, were approved by and conducted in accordance
378 with the Emory University Institutional Animal Care and Use Committee.

379 Mouse tissue fixation

380 Mice were given a lethal dose of isoflurane via inhalation, then transcardially perfused with ice
381 cold 4.0% paraformaldehyde in 0.1M phosphate buffer. Brain and spinal cord were dissected and
382 post fixed in cold paraformaldehyde solution for 2 hours. Brain weights and sizes were taken
383 from mice that were euthanized by cervical dislocation. Brain was dissected, immediately
384 weighed, imaged, and fixed in cold 4.0% paraformaldehyde in 0.1M phosphate buffer overnight.
385 In all cases, tissues were transferred to cold PBS, then serially dehydrated and embedded in
386 paraffin and serially sectioned into 8µm coronal sections.

387 Histology and histological studies

388 Hematoxylin and eosin staining was performed according to standard procedures. Briefly,
389 sections were dewaxed with xylenes and serial ethanol dilutions then stained with Eosin using
390 the Richard-Allan Scientific Signature Series Eosin-Y package (ThermoScientific). To derive
391 unbiased estimates of neuronal loss in the hippocampus, the number of primordial neurons in

392 CA1 and CA3 (corresponding approximately to bregma coordinates -2.0 mm and -3.0 mm) were
393 counted from 2 randomly selected regions in the field of a Zeiss Axiophot ocular graticule grid
394 and measured manually using digital micrographs of H&E-stained preparations. Investigators
395 were blinded to the genotype or treatment.

396 Immunohistochemistry and immunofluorescence

397 Sections were dewaxed with xylenes and serial ethanol dilutions, then treated with 3% hydrogen
398 peroxide at 40°C for 5 minutes to quench endogenous peroxidase activity, blocked in 2% serum
399 at 40°C for 15 minutes, and incubated with primary Ab (Table S1) overnight at 4°C. Slides were
400 washed, then incubated with biotinylated secondary Ab (Biotinylated Goat α Rabbit, 1:200,
401 Vector Labs BA-1000 or Biotinylated Goat α Mouse, 1:200, Vector Labs BA-9200) at 37°C for
402 30 minutes. Signal amplification was then carried out by incubating at 37°C for 1 hour with
403 Vector Labs Elite ABC reagent (PK-6200). Slides were developed with DAB for 1-5 minutes,
404 counterstained with hematoxylin for 1 minutes, and coverslipped. For immunofluorescence,
405 dewaxed sections were first rinsed with TBS. Antigen retrieval was performed by microwaving
406 at 10% power 2X for 5 minutes in 0.01M sodium citrate. Slides were then cooled, washed with
407 TBS, permeabilized in 0.5% Triton X-100 for 20 minutes, followed by blocking in 10% goat
408 serum 20 minutes. Primary Abs (Table S1) were incubated overnight at 4°C. Slides were then
409 washed and incubated in secondary Abs (Invitrogen A1 1001 and Invitrogen A11012) for 1 hour
410 at room temperature, followed by TBS washes, counterstained with DAPI, and then
411 coverslipped. For the assessment of tau accumulation, six random sections (sampling from CA1,
412 CA3, and cerebral cortex) per sample were manually counted using digital micrographs of AT8
413 stained preparations in the field of a Zeiss Axiophot ocular graticule grid. Investigators were
414 blinded to the genotype or treatment. Imagining for immunofluorescence of LSD1 staining was

415 performed on a spinning-disk confocal Nikon-Tie controlled with the software NIS Elements
416 (Nikon). Imaging for all other immunofluorescence staining was performed on an Eclipse Ti2
417 inverted microscope (Nikon, Toyko, Japan) controlled with the software NIS Elements (Nikon).
418 Image J software ((NIH, http://imagej.nih.gov/ij/) was used for viewing all images.

419 Protein Quantification

420 Protein levels were determined by homogenizing brains in 1 ml/g of tissue in ice-cold lysis
421 buffer (150mM NaCl, 1% Triton X-100, 0.5% Na-deoxycholate, 1% SDS, 50mM Tris, pH8.0) in
422 a dounce homogenizer, followed by end-over-end spin at 4°C for 2 hours, and centrifugation at
423 20,000 x g for 20 minutes at 4°C. Protein concentrations were determined following standard
424 BCA protocol (Pierce BCA Protein Assay Kit). Equal amounts of protein for each sample were
425 loaded and run on a 12% SDS-PAGE gel, transferred (Semi-dry transfer using BIO RAD Trans-
426 Blot Turbo Transfer System), blocked in 5% BSA, and probed with primary Ab (Table S1) over
427 night at 4°C. Blots were rinsed and stained with HRP-conjugated secondary Ab, and detected by
428 chemiluminescence using ChemiDoc MP Imaging System (BIO RAD). Protein levels were
429 normalized using total protein calculated using BIO RAD ImageLab software.

430 Quantitative analysis of paralysis

431 We performed experiments on PS19 Tau, *Lsd1*$^{\Delta/+}$, PS19;*Lsd1*$^{\Delta/+}$ mice at 6, 8, and 10 months.
432 For the rotarod experiments, mice were given two practice trials and then placed on the rotating
433 cylinder at 4rpm. Rotational speed then gradually increased over a 5-minute test session up to a
434 maximum rotational speed of 40rpm. Latency to fall off of the accelerating rotarod was used as
435 the dependent variable. We calculated the latency to fall, maximum speed in rotations per
436 minute, and distance traveled. For grid performance, mice were placed on a horizontal grid that

437 was then inverted so mice are hanging upside down by their paws. Mice were videotaped for 10
438 seconds, and then scored for forepaw and back paw distance traveled. Mice that could not hold
439 onto grid for 10 seconds were censored. Investigators were blinded to the genotypes for both
440 experiments.

441 MRI of brain atrophy

442 MRI studies were conducted on PS19 Tau, *Lsd1*$^{\Delta/+}$, PS19;*Lsd1*$^{\Delta/+}$ mice at 6 months and 10
443 months (*n*=3/genotype). Mice were anesthetized with isoflurane, and monitored for heart rate and
444 temperature changes while anesthetized. MRI measurements were performed using a 9.4 T/20
445 cm horizontal bore Bruker magnet, interfaced to an AVANCE console (Bruker, Billerica, MA,
446 USA). A two-coil actively decoupled imaging set-up was used (a 2 cm diameter surface coil for
447 reception and a 7.2 cm diameter volume coil for transmission). Axial T2-weighted images were
448 acquired with a RARE (Rapid Acquisition with Refocused Echos) sequence. Its imaging
449 parameters were as follows: TR = 3000 ms, Eff.TE = 64 ms, RARE factor = 4, field of view
450 (FOV) = 23.04 × 23.04 mm2, matrix = 192 × 192, Avg = 4, slice thickness (thk) = 0.6 mm,
451 number of slice(NSL)=20. Specific emphasis was placed on the neocortex and hippocampus in
452 the coronal images (1.0 – 4.0 mm posterior to the bregma).

453 RNA sequencing

454 9 month old *Lsd1*$^{+/+}$, *Lsd1*$^{\Delta/+}$, PS19 Tau, and PS19;*Lsd1*$^{\Delta/+}$ littermates (n=2 mice/genotype)
455 were euthanized by cervical dislocation, hippocampi were dissected and snap frozen with liquid
456 nitrogen in 1mL Trizol, and stored at -80°C. For RNA isolation, samples were thawed at 37°C
457 then kept on ice prior to homogenization with Polytron homogenizer with a 5 second pulse. After
458 a 5 minute incubation at room temperature, one tenth the sample volume of 1-bromo-
459 3chloropropane was added, mixed by inversion and incubated for 3 minutes at room temperature.

460 Samples were then centrifuged at 13,000 X g for 15 minutes at 4°C to separate the aqueous and
461 organic layers. As much of the aqueous layer was recovered as possible, then RNA was
462 precipitated with isoproponal. Pellets were then washed with 75% ethanol and resuspended in
463 50µL of dionized water. RNA library preparation and sequencing were performed by
464 HudsonAlpha Genomic Services Lab. RNA was Poly(A) selected and 300bp size selected.
465 Libraries were sequenced for 25 million 50bp paired end reads.

466 RNA sequencing analysis

467 The sequencing data were uploaded to the Galaxy web platform, and *we used the public server*
468 *at* usegalaxy.org *to analyze the data ((45, 46)).* FASTQ files were quality assessed using
469 FASTQC (v.0.11.7), trimmed using Trimmomatic (v.0.36.5) and minimum QC score of 20 and
470 minimum read length of 36bp. Paired-end reads were subsequently mapped to the GRCm38
471 genome using HISAT2 (v.2.1.0). Unmapped, unpaired and multiply mapped reads were removed
472 using Filter SAM or BAM (v.1.1.2). Assignment of transcripts to GRCm38 genomic features
473 was performed using Featurecounts (v.1.6.0.6) and the Ensembl GRCm38.93 gtf file.
474 Differentially expressed transcripts were determined using DESEQ2 (v.2.11.40.2) (*(46))*. For all
475 datasets, a cutoff of adjusted p-value < 0.3 and abs ($\log_2$ fold change) > 0.58 was applied. TPM
476 values were calculated from raw data obtained from Featurecounts output. Subsequent
477 downstream analysis was performed using R and normalized counts and adjusted P-values from
478 DESEQ2 (v.2.11.40.2). Heatmaps were produced and hierarchical clustering was done using the
479 gplots package (v. 3.0.1) and normalized counts (*(47)*). Volcano plots were produced using the
480 enhanced volcano package (v.0.99.16) and adjusted p-values (*(48)*). Additionally, Gene Set
481 Enrichment Analysis (Pre-ranked list) was performed using the online platform WebGestalt (*(49-*
482 *52))*. Custom R-scripts available upon request.

483 Stereotaxic surgery and viral infusion

484 All surgical procedures were approved by and conducted in accordance with the Emory
485 University Institutional Animal Care and Use Committee. Mice were anesthetized with
486 isoflurane (3% induction, 1-2% maintenance) and administered the analgesic meloxicam (5
487 mg/kg). Using a Stoeling Quintessential Stereotaxic Injector pump and Hamilton syringe, mice
488 were injected with either the AAV-DJ-LSD1- HA virus or the control AAV-DJ- HA virus into
489 both hippocampi. Each virus was injected into the rostral (AP: -2.5, ML:± 2.2, DV: -1.6, relative
490 to bregma) and caudal (AP: -3.1, ML:± 3.0, DV: -3.5) hippocampus of both hemispheres (four
491 injection sites total). Infusion volumes were 0.5 µL per injection site, administered at a rate of
492 0.15 µL/min. Following surgery, mice were monitored daily for the duration of the experiment.
493 Brains were extracted 3 months post-surgery which allows sufficient time for viral expression.
494 Injection accuracy was confirmed by HA positive staining, and those mice where staining was
495 outside the hippocampus or that did not fully reach hippocampus were censored.

496

497 **REFERENCES**

498 1. M. E. Orr, A. C. Sullivan, B. Frost, A Brief Overview of Tauopathy: Causes,
499 Consequences, and Therapeutic Strategies. *Trends in pharmacological sciences* **38**, 637-
500 648 (2017).
501 2. Y. Wang, E. Mandelkow, Tau in physiology and pathology. *Nat Rev Neurosci* **17**, 5-21
502 (2016).
503 3. D. M. Holtzman *et al.*, Tau: From research to clinical development. *Alzheimers Dement*
504 **12**, 1033-1039 (2016).
505 4. C. M. Wischik *et al.*, Isolation of a fragment of tau derived from the core of the paired
506 helical filament of Alzheimer disease. *Proc Natl Acad Sci U S A* **85**, 4506-4510 (1988).
507 5. M. Goedert, C. M. Wischik, R. A. Crowther, J. E. Walker, A. Klug, Cloning and
508 sequencing of the cDNA encoding a core protein of the paired helical filament of
509 Alzheimer disease: identification as the microtubule-associated protein tau. *Proc Natl*
510 *Acad Sci U S A* **85**, 4051-4055 (1988).
511 6. J. Hardy, D. J. Selkoe, The amyloid hypothesis of Alzheimer's disease: progress and
512 problems on the road to therapeutics. *Science* **297**, 353-356 (2002).
513 7. S. H. Barage, K. D. Sonawane, Amyloid cascade hypothesis: Pathogenesis and
514 therapeutic strategies in Alzheimer's disease. *Neuropeptides* **52**, 1-18.

515 8. G. S. Bloom, Amyloid-β and Tau: The Trigger and Bullet in Alzheimer Disease
516 PathogenesisAmyloid-β and TauAmyloid-β and Tau. *JAMA Neurology* **71**, 505-508
517 (2014).
518 9. C. Duyckaerts, B. Delatour, M.-C. Potier, Classification and basic pathology of
519 Alzheimer disease. *Acta Neuropathologica* **118**, 5-36 (2009).
520 10. P. V. Arriagada, J. H. Growdon, E. T. Hedley-Whyte, B. T. Hyman, Neurofibrillary
521 tangles but not senile plaques parallel duration and severity of Alzheimer's disease.
522 *Neurology* **42**, 631-639 (1992).
523 11. E. Karran, M. Mercken, B. De Strooper, The amyloid cascade hypothesis for Alzheimer's
524 disease: an appraisal for the development of therapeutics. *Nat Rev Drug Discov* **10**, 698-
525 712 (2011).
526 12. T. Gomez-Isla *et al.*, Neuronal loss correlates with but exceeds neurofibrillary tangles in
527 Alzheimer's disease. *Ann Neurol* **41**, 17-24 (1997).
528 13. A. Bejanin *et al.*, Tau pathology and neurodegeneration contribute to cognitive
529 impairment in Alzheimer's disease. *Brain* **140**, 3286-3300 (2017).
530 14. D. P. Hanger, J. C. Betts, T. L. Loviny, W. P. Blackstock, B. H. Anderton, New
531 phosphorylation sites identified in hyperphosphorylated tau (paired helical filament-tau)
532 from Alzheimer's disease brain using nanoelectrospray mass spectrometry. *J Neurochem*
533 **71**, 2465-2476 (1998).
534 15. M. Morishima-Kawashima *et al.*, Hyperphosphorylation of tau in PHF. *Neurobiol Aging*
535 **16**, 365-371; discussion 371-380 (1995).
536 16. T. Arendt, J. T. Stieler, M. Holzer, Tau and tauopathies. *Brain Research Bulletin* **126**,
537 238-292 (2016).
538 17. R. J. Castellani, G. Perry, Tau Biology, Tauopathy, Traumatic Brain Injury, and
539 Diagnostic Challenges. *J Alzheimers Dis* **67**, 447-467 (2019).
540 18. E. Masliah *et al.*, Altered expression of synaptic proteins occurs early during progression
541 of Alzheimer's disease. *Neurology* **56**, 127-129 (2001).
542 19. M. Ingelsson *et al.*, Early Abeta accumulation and progressive synaptic loss, gliosis, and
543 tangle formation in AD brain. *Neurology* **62**, 925-931 (2004).
544 20. J. W. Kinney *et al.*, Inflammation as a central mechanism in Alzheimer's disease.
545 *Alzheimer's & Dementia: Translational Research & Clinical Interventions* **4**, 575-590
546 (2018).
547 21. J. M. Rubio-Perez, J. M. Morillas-Ruiz, A review: inflammatory process in Alzheimer's
548 disease, role of cytokines. *TheScientificWorldJournal* **2012**, 756357-756357 (2012).
549 22. H. Braak, D. R. Thal, E. Ghebremedhin, K. Del Tredici, Stages of the pathologic process
550 in Alzheimer disease: age categories from 1 to 100 years. *J Neuropathol Exp Neurol* **70**,
551 960-969 (2011).
552 23. H. Braak, K. Del Tredici, The pathological process underlying Alzheimer's disease in
553 individuals under thirty. *Acta Neuropathol* **121**, 171-181 (2011).
554 24. D. E. Hurtado *et al.*, A{beta} accelerates the spatiotemporal progression of tau pathology
555 and augments tau amyloidosis in an Alzheimer mouse model. *Am J Pathol* **177**, 1977-
556 1988 (2010).
557 25. Z. He *et al.*, Amyloid-beta plaques enhance Alzheimer's brain tau-seeded pathologies by
558 facilitating neuritic plaque tau aggregation. *Nat Med* **24**, 29-38 (2018).
559 26. S. H. Choi *et al.*, A three-dimensional human neural cell culture model of Alzheimer/'s
560 disease. *Nature* **515**, 274-278 (2014).

561 27. H. Braak, E. Braak, Frequency of Stages of Alzheimer-Related Lesions in Different Age
562 Categories. *Neurobiology of Aging* **18**, 351-357 (1997).
563 28. M. A. Christopher *et al.*, LSD1 protects against hippocampal and cortical
564 neurodegeneration. *Nature Communications* **8**, 805 (2017).
565 29. Y. Yoshiyama *et al.*, Synapse Loss and Microglial Activation Precede Tangles in a
566 P301S Tauopathy Mouse Model. *Neuron* **53**, 337-351.
567 30. A. Bellucci *et al.*, Induction of Inflammatory Mediators and Microglial Activation in
568 Mice Transgenic for Mutant Human P301S Tau Protein. *The American Journal of*
569 *Pathology* **165**, 1643-1652 (2004).
570 31. M. Iba *et al.*, Tau pathology spread in PS19 tau transgenic mice following locus
571 coeruleus (LC) injections of synthetic tau fibrils is determined by the LC's afferent and
572 efferent connections. *Acta Neuropathol* **130**, 349-362 (2015).
573 32. C. T. Foster *et al.*, Lysine-specific demethylase 1 regulates the embryonic transcriptome
574 and CoREST stability. *Molecular and cellular biology* **30**, 4851-4863 (2010).
575 33. L. Jin *et al.*, Loss of LSD1 (lysine-specific demethylase 1) suppresses growth and alters
576 gene expression of human colon cancer cells in a p53- and DNMT1(DNA
577 methyltransferase 1)-independent manner. *The Biochemical journal* **449**, 459-468 (2013).
578 34. D. B. Lyons *et al.*, An epigenetic trap stabilizes singular olfactory receptor expression.
579 *Cell* **154**, 325-336 (2013).
580 35. B. I. Giasson, W. E. Mushynski, Aberrant stress-induced phosphorylation of perikaryal
581 neurofilaments. *J Biol Chem* **271**, 30404-30409 (1996).
582 36. Y. L. Liu *et al.*, Alternation of neurofilaments in immune-mediated injury of spinal cord
583 motor neurons. *Spinal Cord* **47**, 166 (2008).
584 37. L. D. F. Moon, Chromatolysis: Do injured axons regenerate poorly when ribonucleases
585 attack rough endoplasmic reticulum, ribosomes and RNA? *Dev Neurobiol* **78**, 1011-1024
586 (2018).
587 38. B. G. Cragg, What is the signal for chromatolysis? *Brain Res* **23**, 1-21 (1970).
588 39. S. Sil, A. R. Goswami, G. Dutta, T. Ghosh, Effects of naproxen on immune responses in
589 a colchicine-induced rat model of Alzheimer's disease. *Neuroimmunomodulation* **21**, 304-
590 321 (2014).
591 40. J. Riancho *et al.*, Compensatory Motor Neuron Response to Chromatolysis in the Murine
592 hSOD1(G93A) Model of Amyotrophic Lateral Sclerosis. *Front Cell Neurosci* **8**, 346
593 (2014).
594 41. A. M. Cataldo, D. J. Hamilton, R. A. Nixon, Lysosomal abnormalities in degenerating
595 neurons link neuronal compromise to senile plaque development in Alzheimer disease.
596 *Brain Res* **640**, 68-80 (1994).
597 42. B. Eftekharzadeh *et al.*, Tau Protein Disrupts Nucleocytoplasmic Transport in
598 Alzheimer's Disease. *Neuron* **99**, 925-940.e927 (2018).
599 43. L. G. Sheffield, H. B. Miskiewicz, L. B. Tannenbaum, S. S. Mirra, Nuclear Pore
600 Complex Proteins in Alzheimer Disease. *Journal of Neuropathology & Experimental*
601 *Neurology* **65**, 45-54 (2006).
602 44. B. Frost, F. H. Bardai, M. B. Feany, Lamin Dysfunction Mediates Neurodegeneration in
603 Tauopathies. *Curr Biol* **26**, 129-136 (2016).
604 45. E. Afgan *et al.*, The Galaxy platform for accessible, reproducible and collaborative
605 biomedical analyses: 2016 update. *Nucleic Acids Res* **44**, W3-w10 (2016).

606 46. E. Afgan *et al.*, The Galaxy platform for accessible, reproducible and collaborative
607 biomedical analyses: 2018 update. *Nucleic Acids Research* **46**, W537-W544 (2018).
608 47. B. B. Gregory R. Warens, Lodewijk Bonebakker, Robert Gentleman, Wolfgang Huber
609 Andy Liaw, Thomas Lumley, Martin Maechler, Arni Magnusson, Steffen Moeller, Marc
610 Schwartz, Bill Venables. (2019).
611 48. K. Blighe, in *R. package version 1.2.0*. (2019).
612 49. J. Wang, D. Duncan, Z. Shi, B. Zhang, WEB-based GEne SeT AnaLysis Toolkit
613 (WebGestalt): update 2013. *Nucleic Acids Res* **41**, W77-83 (2013).
614 50. J. Wang, S. Vasaikar, Z. Shi, M. Greer, B. Zhang, WebGestalt 2017: a more
615 comprehensive, powerful, flexible and interactive gene set enrichment analysis toolkit.
616 *Nucleic Acids Res* **45**, W130-w137 (2017).
617 51. Y. Liao, J. Wang, E. J. Jaehnig, Z. Shi, B. Zhang, WebGestalt 2019: gene set analysis
618 toolkit with revamped UIs and APIs. *Nucleic Acids Res* **47**, W199-w205 (2019).
619 52. B. Zhang, S. Kirov, J. Snoddy, WebGestalt: an integrated system for exploring gene sets
620 in various biological contexts. *Nucleic Acids Res* **33**, W741-748 (2005).

621

622 **ACKNOWLEDGMENTS**

623 We thank M. Rosenfeld (U.C.S.D) for providing *Lsd1* deletion mice; N. Seyfried, R. Betarbet,
624 Mr. Gearing, from the Emory ADRC (P50 AG025688), NINDS Emory Neuroscience Core
625 Facilities (P30NS055077) for tissue processing and providing PHF1 antibody, J. Alcudia of the
626 Stanford Gene Vector and Virus Core for the help with virus generation and production; J.
627 Schroeder from Emory Rodent Behavioral Core for help with Rotatord and Grid Performance
628 assays supported by the Emory Neuroscience NINDS Core Facilities (P30NS055077) with
629 further support provided by the Georgia Clinical & Translational Science Alliance of the
630 National Institutes of Health under Award Number UL1TR002378; and J. Park from the Emory
631 Center for Systems Imagining for preforming MRI supported by the National Center for
632 Advancing Translational Sciences of the National Institutes of Health under Award Number
633 UL1TR000454**.** We would also like to thank M.J. Rowley and V. Corces for assistance on RNA
634 sequencing analysis, K. Porter-Stransky and D. Weinshenker for providing PS19 Tau mouse and
635 teaching stereotaxic surgery procedure, L.R. Lym and Dr. Lerit for assistance with confocal
636 imagining; D. Weinshenker, A. Levey, C. Bean and T. Caspary for comments on the manuscript

637 and assistance throughout. Additionally the authors would like to thank fellow Katz lab members
638 for assistance experimentally and intellectually. **Funding:** A.K.E was supported by the National
639 Institute of General Medicine training grant (T32 GM008367-26) and an NRSA from National
640 Institute of Neurological Disorders and Stroke (NINDS) (F31 NS098663-02). D.A.M was
641 supported by a research supplement to promote diversity in health-related research from the
642 NINDS (1R01NS087142). S.M.K was supported the NINDS Training in Translational Research
643 in Neurology grant (5T32 NS007480-17). The work was supported by a grant to D.J.K from the
644 National Institute of Neurological Disorders and Stroke (1R01NS087142). **Author**
645 **Contributions:** A.K.E and D.J.K. conceived and designed the study and wrote the manuscript.
646 A.K.E. performed experiments with the help of A.C.W, S.M.K, and R.A.M under the direction
647 of D.J.K. D.A.M performed bioinformatics analysis on the RNA sequencing data. A.K.E,
648 A.C.W, S.M.K, and R.A.M analyzed all other data and interpreted results. All authors discussed
649 the results and commented on the manuscript. **Competing Interests:** The authors declare that
650 they have no competing interests. **Data and materials availability:** FastQ files for the RNA
651 sequencing experiments are bring deposited in the GEO and will be available upon publication.
652 Results from DESEQ2 are available in Data S1. Correspondence and requests for materials
653 should be addressed to D.J.K. (djkatz@emory.edu).
654

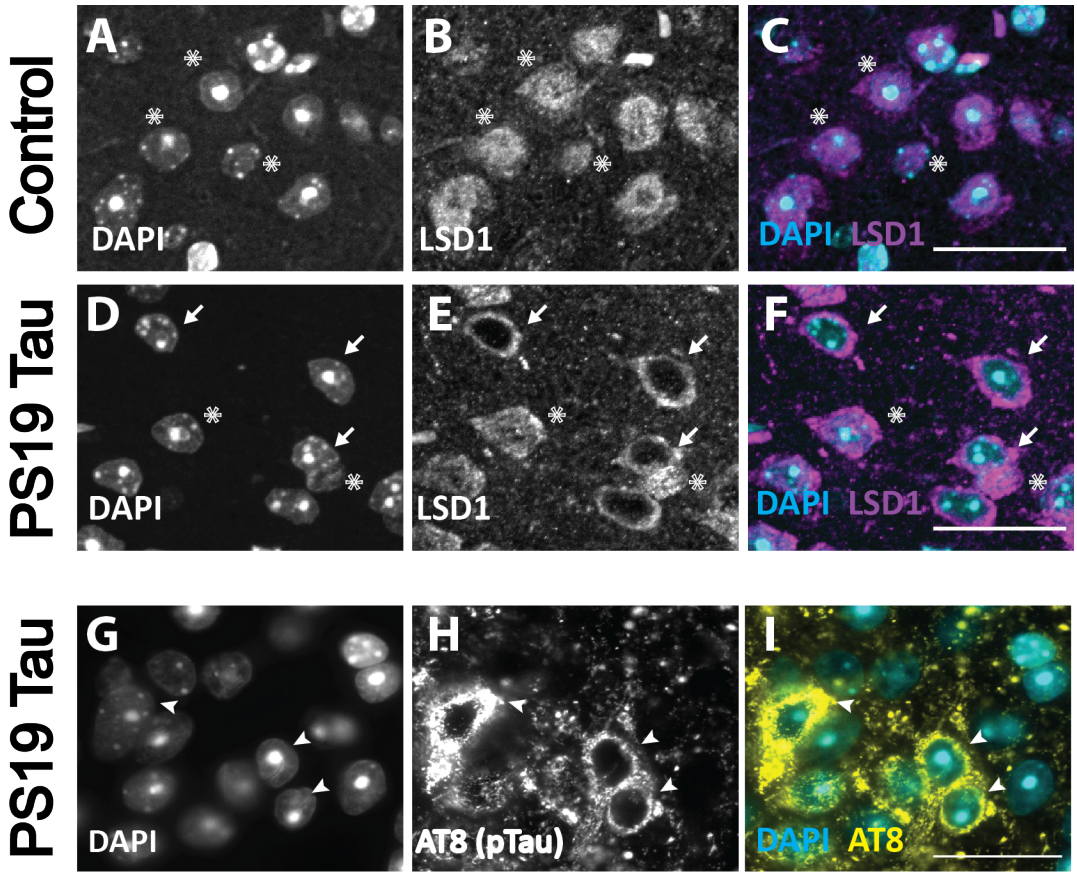

Fig. 1: LSD1 sequestration and tau accumulation in PS19 Tau mice. A-C, Representative immunofluorescence of 12 month old control Wild Type mice showing DAPI (**A**), LSD1 (**B**), and merged (**C**) in the cerebral cortex where LSD1 is localized specifically to DAPI positive nuclei. **D-F**, Representative image of the cerebral cortex in 12 month old PS19 Tau mice. Staining for DAPI (**D**), LSD1 (**E**), and merged (**F**) shows that LSD1 is localized outside the nucleus, and depleted from the DAPI positive nucleus. Arrows denote cells where LSD1 is localized outside of the nucleus, and asterisks denote LSD1 localized specifically to the nucleus. **G-I,** Representative immunofluorescence of 12 month old PS19 Tau mouse with staining for DAPI (**G**), AT8 positive hyper-phosphorylated tau (**H**) and merge (**I**) where hyper-phosphorylated tau accumulates in the cytoplasm of the cell body. Arrowheads denote hyper-phosphorylated tau. Scale bars=25µm.

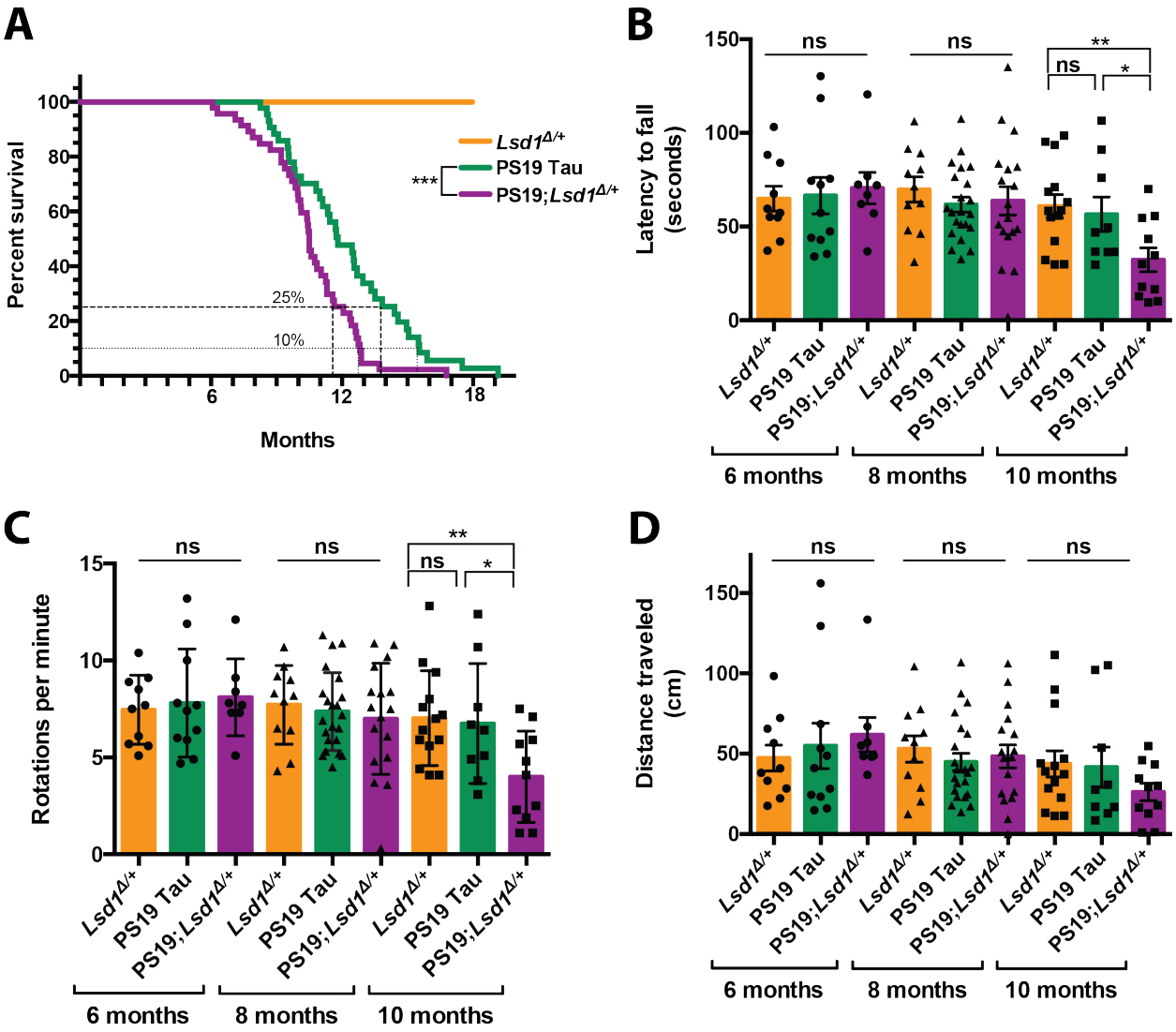

Fig. 2: Reduction of *Lsd1* exacerbates the PS19 Tau mouse paralysis phenotype. A, Lifespan curve showing that no *Lsd1*$^{\Delta/+}$ mice died before 18 months (orange, *n*=20). PS19;*Lsd1*$^{\Delta/+}$ mice (purple, *n*=44) have a significant reduction in survival compared to PS19 Tau mice with wild-type levels of *Lsd1* (green, *n*=37)(Log-rank Mantle-Cox test ***P<0.005). **B-D**, Rotarod testing of latency to fall (in seconds) (**B**), rotations per minute (when the mouse fell) (**C**), and distance traveled (in centimeters) (**D**) for mice at age 6, 8 and 10 months. *Lsd1*$^{\Delta/+}$ (orange, *n*=10,11,14), PS19 Tau (green, *n*=11,22,9), and PS19;*Lsd1*$^{\Delta/+}$ (purple, *n*=8,17,11). Values are mean ± SEM (two-way analysis of variance (ANOVA) with Tukey's post hoc test *P<0.05 **P<0.01, ns=not significant).

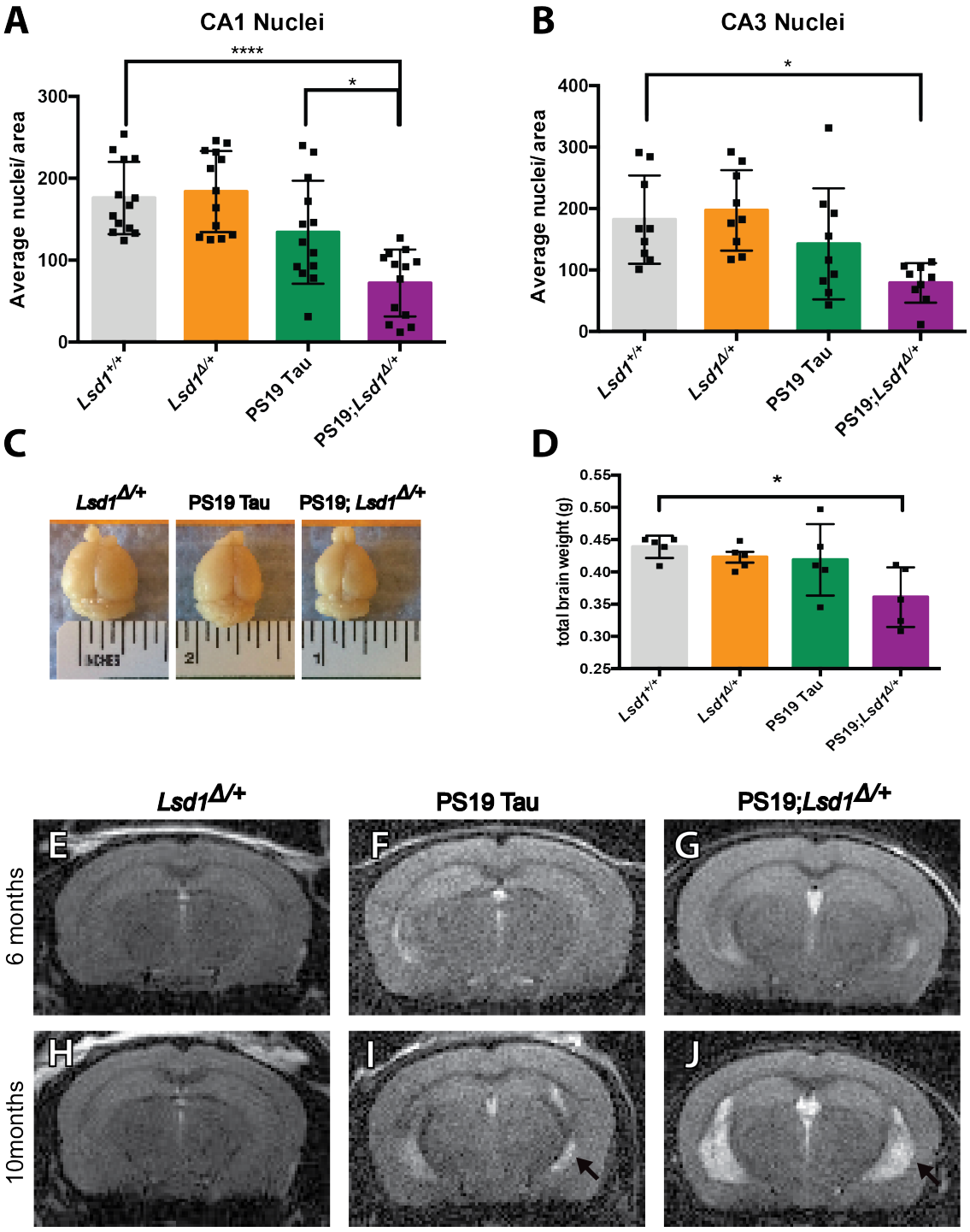

Fig. 3: Reduction of *Lsd1* exacerbates neurodegeneration in PS19 Tau mice. A,B, Average nuclei per area in the CA1 (**A**) and CA3 (**B**) regions of the hippocampus in 12 month old *Lsd1*$^{+/+}$, *Lsd1*$^{\Delta/+}$, PS19 Tau, and PS19;*Lsd1*$^{\Delta/+}$ mice. Quantification from histology represented in **Fig. S5 A-H**. Values are mean ± SD (**A**, *n*=13 & **B,** *n*=9). **C,** Representative image of the brains of 12 month old *Lsd1*$^{\Delta/+}$, PS19 Tau, and PS19;*Lsd1*$^{\Delta/+}$ littermates. **D,** Total brain weight of 12 month old littermates represented in **Fig. 3C.** Values are mean ± SD (*n*=5). For all graphs: one-way analysis of variance (ANOVA) with Tukey's post hoc test (two-sided) *P<0.05,****P<0.001. **E-J,** Representative image of T2- weighted RARE coronal MRI taken from 6 months (**E-G**) and 10 months (**H-jJ**) of age in *Lsd1*$^{\Delta/+}$ (**E,H**), PS19 (**F,J**), and PS19;*Lsd1*$^{\Delta/+}$ (**G,J**) mice (*n*=3). Arrow denotes region of hippocampal atrophy.

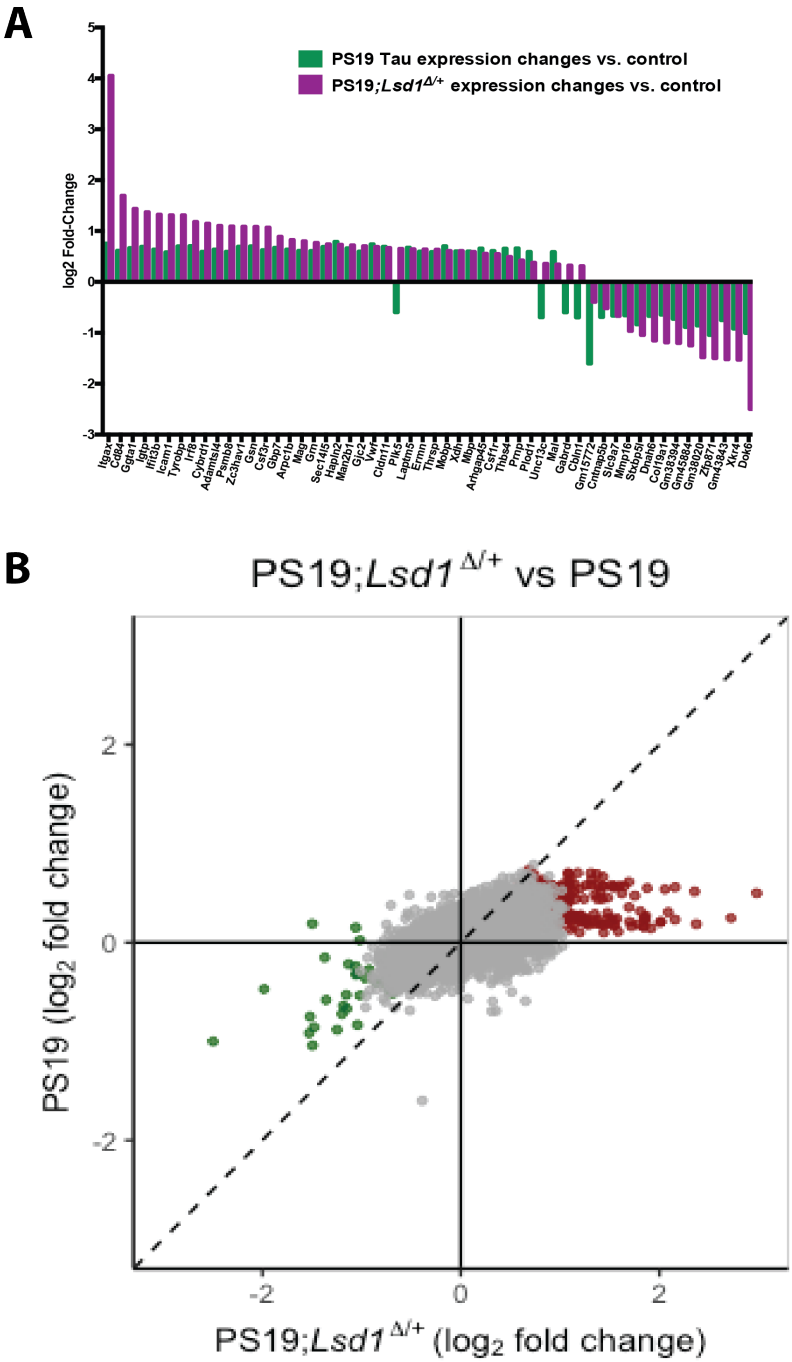

Fig. 4: Molecular overlap between loss of LSD1 function and tauopathy. A, Histogram ($\log_2$ fold change) of the 54 genes that have significant changes in expression in the PS19 Tau mouse (green) and their corresponding expression changes in the PS19;*Lsd1*$^{\Delta/+}$ mouse (purple). **B,** Scatter plot showing the correlation between the genome-wide $\log_2$ fold change in gene expression between PS19 Tau and PS19;*Lsd1*$^{\Delta/+}$. The most significantly changed genes in PS19;*Lsd1*$^{\Delta/+}$ mouse are shown in red (upregulated) and green (downregulated). All other genes are shown in grey. Dotted line represents 1:1 relationship between gene expression changes in PS19 Tau vs. PS19;*Lsd1*$^{\Delta/+}$. Exacerbated genes fall to the right of the dotted line in the positively correlated quadrant and to the left of the dotted line in the negatively correlated quadrant. Genes with correlated expression changes are found in the top right and bottom left quadrants, while genes that do not correlate are found in the opposite quadrants.

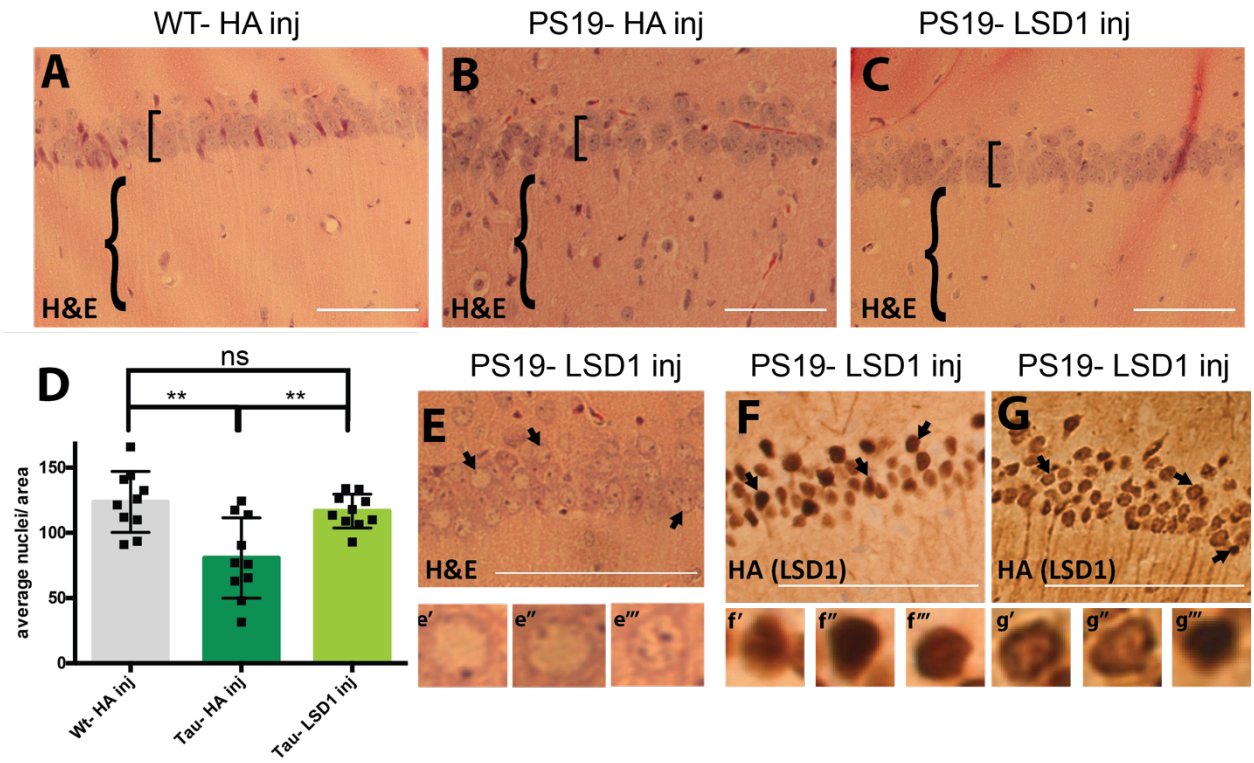

Fig. 5: LSD1 overexpression rescues the neurodegenerative phenotype in the hippocampus of 11 month old PS19 Tau mice. A-C, Representative image of H&E stained CA1 region of the hippocampus of 11 month old Wild Type mice injected with HA control virus (WT- HA inj) (**A**), PS19 Tau mice injected with HA control virus (PS19-HA inj) (**B**), and PS19 Tau mice injected with *Lsd1* overexpressing virus (PS19- LSD1 inj) (**C**). Square brackets denote thickness of pyramidal layer of the CA1 of the hippocampus and curvy brackets denote hippocampal region with or without infiltrating cells. **D,** Quantification of the average number of nuclei in the pyramidal layer of the hippocampus per area per mouse from histology represented in **Fig. 5A-C**. Values are mean ± SD (n=10, one-way analysis of variance (ANOVA) with Tukey's post hoc test, **$p<0.01$, ns=not significant). **E,** Representative H&E of PS19- LSD1 inj mouse with abnormal nuclei blebbing in the CA1 region of the hippocampus. **E'-E'''**, High magnified image of cells denoted by arrows in **Fig. 5E** of individual nuclei that are either abnormally blebbed (**E', E"**) or normal (**E'''**). **F,G,** Immunohistochemistry staining of HA(LSD1) in 11 month PS19- LSD1 inj mice. HA is either localized specifically to the nucleus in all nuclei (**F**) or in only a few nuclei while it is partially sequestered in the cytoplasm in others (**G**). **F'-F'''**, High magnified image of cells denoted by arrows in **Fig. 5F** of nuclear HA localization in individual nuclei. **G'-G'''**, High magnified image of cells denoted by arrows in **Fig. 5G** of individual nuclei with HA(LSD1) either sequestered to the cytoplasm (**G', G"**) or confined to the nucleus (**G'''**). Scale bars=50µm.